

Dark Matter through a Superconductivity Analogy: From Model to Cosmology.

Undergraduate Honors Thesis.

Fernando Garcia Cortez

Research advisor: Francis-Yan Cyr-Racine.



THE UNIVERSITY OF
NEW MEXICO.

Albuquerque, NM
May 11th, 2025

Contents

| | |
|--|-----------|
| Abstract | 2 |
| Acknowledgments | 3 |
| 1 Introduction: The Current State of Cosmology | 4 |
| 1.1 Our Universe | 4 |
| 1.1.1 The Cosmological Principle and Expansion | 4 |
| 1.1.2 Ingredients | 5 |
| 1.1.3 Cosmological Observables: the Universe’s Blueprint | 7 |
| 1.1.4 Dark matter and Λ CDM | 9 |
| 1.2 Moving beyond CDM: prelude to SCDM | 9 |
| 2 Superconducting Dark Matter | 11 |
| 2.1 Theory | 11 |
| 2.2 Scalar characterization | 13 |
| 2.3 Cosmological Evolution | 17 |
| 3 Cosmological Impacts of SCDM | 21 |
| 3.1 CLASS and Its Modifications | 21 |
| 3.2 Background Quantities | 24 |
| 3.3 Matter Power Spectrum | 25 |
| 3.4 Impacts on the CMB | 26 |
| 4 Conclusion and Future Work | 28 |
| Bibliography | 29 |
| Appendix A: Evaluation of Fermi-Dirac integrals | 31 |
| Appendix B: SCDM Data Generation in Python | 33 |

Abstract

Our current cosmological model operates under the assumption that dark matter is cold ($w_{\text{dm}} = 0$). In this work, we challenge this assumption by revisiting a model of dark matter inspired by an analogy to BCS superconductivity, known as superconducting dark matter (SCDM). After reviewing the field-theoretic foundations of the model, we derive the necessary equations to implement it as a fluid in cosmological Boltzmann code solvers, with an emphasis on its decaying properties, which allow for a greater abundance of dark matter in the early universe. Although observations of the matter power spectrum and CMB anisotropies suggest that SCDM predicts enhanced structure formation and anisotropies across all scales, the model generally remains within observational bounds when compared to recent cosmological data. This suggests a possible relaxation of the coldness requirement, inviting the development of new models to further explore the nature of dark matter.

Acknowledgments

I would first like to thank Professor Francis-Yan Cyr-Racine for his support and guidance since our first project together in the summer of 2023. Thank you for teaching me the importance of rigorous and meaningful work, and for welcoming me into the particle cosmology group at UNM. I am also grateful to David, Kylar, and John for their guidance and insight throughout my studies in cosmology.

I would like to thank Professor Rouzbeh Allahverdi for the time we spent working on thermal quantum field theories—work that laid the foundation for this project—as well as for our discussions on the field theory underlying superconducting dark matter.

Finally, I want to thank my parents for their unwavering support of my education at UNM as an international student. It is thanks to their encouragement and sacrifices that I have had the opportunity to complete this research project.

Chapter 1

Introduction: The Current State of Cosmology

1.1 Our Universe

1.1.1 The Cosmological Principle and Expansion

Our universe, much like oceans that appear calm and flat when viewed from a distance, appears uniform and isotropic when observed on the largest scales. In other words, there is no preferred location or direction in which to study the cosmos. This assumption, known as the **cosmological principle**, is one of the foundational pillars of modern cosmology.

It is this large-scale uniformity that allows us to speak of the universe’s constituents in a simplified and meaningful way. When we refer to “matter” in cosmology, we are not concerned with local concentrations—such as stars, galaxies, or clusters—but rather with how matter behaves and distributes across the universe as a whole.

Our universe, from this perspective, is made out of three main ingredients: matter, radiation, and so-called dark energy. One may also speak of curvature as a component that changes the dynamics and evolution of the universe, but in this work we will be working on a spatially-flat universe.

Although flat, our universe is expanding over time [Hub29]. The degree by which our universe expands is quantified through a quantity known as the **scale factor**, $a(t)$. The scale factor measures how the distance between two objects grows as time progresses. The rate of expansion in the universe is commonly referred to as the Hubble parameter:

$$H(t) = \frac{\dot{a}(t)}{a(t)}, \tag{1.1}$$

where a dot represents a derivative with respect to coordinate-time.

In an expanding universe, the wavelengths of photons expand in direct proportion to the scale factor. This is observed as a discrepancy between the wavelength of light emitted by a source and the received wavelength by an observer. Observers will always detect a longer (towards the red-side of the light spectrum) wavelength. We refer to the

(fractional) change in wavelength as the redshift z of a source, and it is given by:

$$z \equiv \frac{\lambda_{\text{received}} - \lambda_{\text{emitted}}}{\lambda_{\text{emitted}}} \quad (1.2)$$

Both the scale factor and redshift provide alternative and useful ways to talk about time in a cosmological context. By normalizing the scale factor to

$$a(t_{\text{today}}) = 1, \quad (1.3)$$

we obtain a dimensionless ruler $a \in (0, 1]$ which, instead of expressing age in units of time, expresses the relative size of the universe at any given moment. When we speak of the universe at scale factor $a = 0.5$, we speak of the time when our universe’s size was half of what it is today. This ruler allows us to use redshift as a time descriptor as well. Since (assuming scale factor normalization)

$$1 + z = \frac{1}{a(t_{\text{emitted}})}, \quad (1.4)$$

A source’s redshift z tells us that the received light was emitted at the time when the universe was $\frac{1}{1+z}$ of its current size.

1.1.2 Ingredients

As discussed earlier, our universe can be described by three main components: matter, radiation, and dark energy. These categories can be defined in several equivalent ways, but the most useful for our purposes is through the **equation of state**,

$$w = \frac{p}{\rho} \quad (1.5)$$

which characterizes the ratio of pressure p and energy density ρ of a *fluid* component of the universe. Conservation of energy and momentum,

$$\nabla_{\mu} T^{\mu}_{\nu} = 0, \quad (1.6)$$

provides an evolution equation for the energy density of a fluid given its equation of state:

$$\frac{\dot{\rho}}{\rho} = -3(1 + w)\frac{\dot{a}}{a}. \quad (1.7)$$

The solution for ρ follows:

$$\rho \propto a^{-3(1+w)}, \quad (1.8)$$

where we observe that the value of w directly sets how the energy density of the fluid *dilutes* over time.

When we speak of **matter**, we refer to a few things: it includes **baryonic matter** (i.e. the stuff we are made of), as well as any other substance that behaves like “matter”: the pressure of the species is much smaller than its energy density [Bau22]. Effectively, the equation of state for matter is $w = 0$, which in turn implies that the energy density scales as

$$\rho_{\text{m}} \propto a^{-3}. \quad (1.9)$$

Dark matter, a component to be justified latter, behaves like *ordinary* matter in the above sense ($w = 0$). What makes it different is how it interacts (or perhaps, how it does not interact): dark matter does not interact electromagnetically, meaning it neither emits nor absorbs light—hence its name and the idea that we “can’t see it”. Dark matter is also likely to not have strong and weak interactions. As such, dark matter can be thought of as matter that interacts only gravitationally.

Radiation, contrary to matter, has a non-negligible amount of pressure. In particular, anything with equation of state $w = 1/3$ is called radiation. The radiation category includes light (low in mass) particles, photons, neutrinos, and any other relativistic species [Bau22]. Conservation of energy and momentum tells us that

$$\rho_r \propto a^{-4} \tag{1.10}$$

Where the extra power of a^{-1} (relative to matter evolution) comes from the fact that relativistic particles get redshifted. As their wavelength increases, their energy ($E = hc/\lambda$) decreases.

Dark energy is characterized by its negative pressure, with $w = -1$ [Bau22]. This equation of state tells us that

$$\rho_{de} \propto a^0 = 1, \tag{1.11}$$

meaning that the energy density never dilutes. If the universe expands, this means that energy has to be created in order to keep ρ_{de} constant. Some candidates for dark energy include vacuum energy (the energy of empty space), a cosmological constant (Λ), and other models where w isn’t always -1, but varying in time.

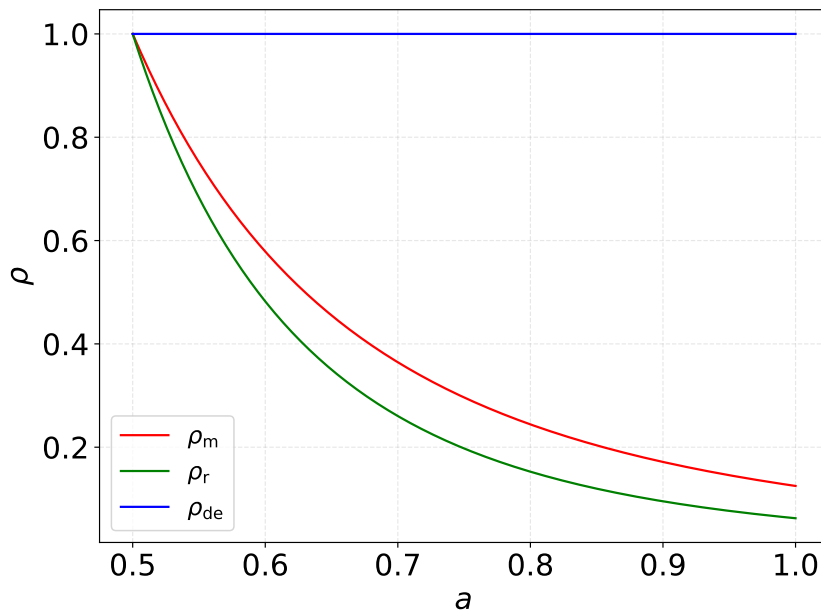


Figure 1.1: Dilution of energy densities. As the universe expands, radiation energy density decays faster than matter, while the energy density of dark energy remains constant. In this example, all three energy densities were set to 1 at $a = 1/2$. When evolved to today ($a = 1$), $\rho_m^{\text{today}} = 1/8$, which is greater than the radiation energy density $\rho_r^{\text{today}} = 1/16$.

1.1.3 Cosmological Observables: the Universe’s Blueprint

The conditions in the early universe did not allow protons and electrons to bond and form even the simplest atom: hydrogen. Instead, the universe was an immense soup of individual particles, constantly flying around and scattering off one another. In particular, photons interacted heavily with free electrons through Thomson scattering [Bau22]. As a result, photons had an extremely short mean free path¹, rendering the universe an opaque, foggy mix of radiation and matter.

Once the temperature dropped to around ~ 3500 K [Bau22, Wei08], the universe entered the **recombination** era², during which conditions allowed protons and electrons to form neutral hydrogen atoms. This led to a substantial drop in the density of free electrons.

Even with a much lower free electron density, photons had one last challenge to overcome before traveling freely through the universe. The photon mean free path wasn’t large enough for them to travel freely. Photons have to overcome the expansion of the universe to travel freely. We quantify this through the Hubble length, H^{-1} , which is the length at which objects recede at the speed of light from each other due to the expansion of the universe.

Once the universe cooled down enough (~ 3000 K), the photon mean free path became larger than the Hubble length, which in combination with an even lower density of free electrons, allowed photons to travel freely through the universe. It is at this point in time, known as **last-scattering**, that the universe became transparent [Bau22]. The **Cosmic Microwave Background** (CMB) represents a picture of the universe at that time. For a while, direct measurements of the CMB seemed to indicate that this faint glow had no anisotropies. We know today that it indeed has anisotropies (as observed by the COBE [COB92], WMAP [WMA03], and PLANCK [Pla14, Pla20a] experiments/collaborations.), implying that the early universe wasn’t completely smooth as we thought [Dod03].

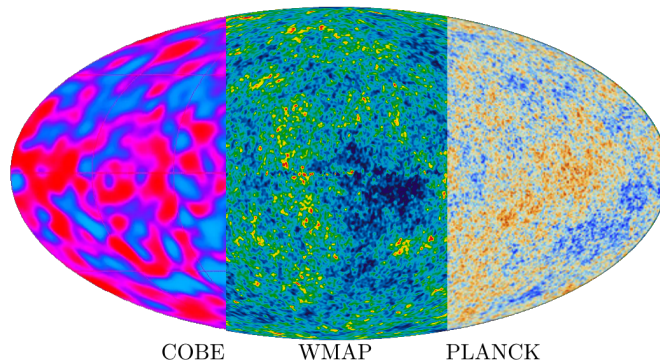


Figure 1.2: Improvements in the observations of CMB anisotropies over time. These color maps represent fluctuations in temperature. COBE had a sensitivity of $\sim 200 \mu\text{K}$, with an angular resolution of ~ 420 arcminutes. WMAP had a sensitivity of $\sim 10 \mu\text{K}$, with an angular resolution of 12 arcminutes. PLANCK had a sensitivity of $\sim 2 - 5 \mu\text{K}$ with an angular resolution of ~ 5 arcminutes. This figure was stitched by the author with no further manipulations.

¹The average distance a particle travels before interacting.

²Despite the name, there was no prior “combination.” The term “recombination” was borrowed from plasma physics.

Before COBE, heat maps of like the ones in Fig. 1.3 were smooth, showing a uniform glow. We are now able to see fluctuations (grainy features) due to improvements in observational equipment.

CMB anisotropies can be quantified through an angular power spectrum. By decomposing temperature variations into spherical harmonics, we are able to write down *amplitudes* of fluctuations as a function of angular scale.

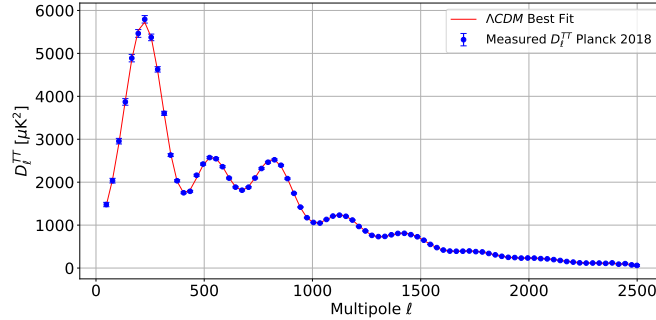


Figure 1.3: Planck TT Power Spectra. Blue points with error bars show the measured temperature fluctuations by the Planck collaboration in 2018. The red curve is a computed spectra for a Λ CDM model that best fits the Planck 2018 data.

Spectra come in different types. In this work we will focus on the **TT** (temperature-temperature) CMB power spectrum, which measures correlations in temperature fluctuations.

These small fluctuations in the CMB were amplified over time as the universe evolved, eventually giving rise to the large-scale structure we observe today. Galaxies, clusters, and cosmic filaments all trace their origins back to these primordial perturbations. To study the distribution of matter on cosmic scales, we turn to another key observable: the **matter power spectrum** (MPS). Just as the CMB’s TT power spectrum quantifies the amplitude of temperature fluctuations across different angular scales, the MPS measures the amplitude of matter density fluctuations as a function of spatial scale in the late-time universe.

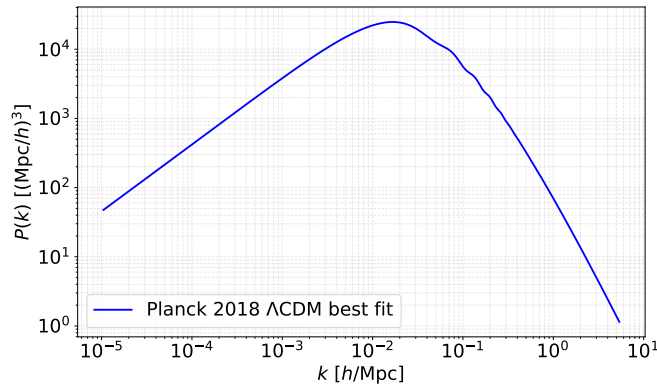


Figure 1.4: Matter Power Spectra for best fit Λ CDM universe. This matter power spectra was computed assuming a Λ CDM universe, using the best fit parameters found by [Pla20a].

Contrary to CMB spectra, the MPS of the universe is not something we can measure directly. Instead, we use statistical inference on large-scale structure surveys (for example, DESI), with the caveat that one must assume a cosmological model beforehand.

1.1.4 Dark matter and Λ CDM

Numerous cosmological and astrophysical observations suggest the presence of more matter than can be observed. As a first example, anisotropy surveys of the CMB can distinguish contributions from regular (baryonic) matter and dark matter. Looking at the matter density $\Omega_m h^2 = 0.1430 \pm 0.0011$ found in [Pla20b], the greatest contribution comes from dark matter: $\Omega_c h^2 = 0.1200 \pm 0.0012$.

Large-scale structure also provides compelling evidence for dark matter. It was shown in [TS04] that the distribution of galaxies, as observed by the Sloan Digital Sky Survey (SDSS), matches the predictions of a universe that includes cold dark matter.

These are just two among many observations that support the existence of dark matter. Others include galaxy cluster dynamics [Zwi37], galaxy rotation curves [Rub80], and gravitational lensing in merging clusters [Clo06]. Despite this indirect evidence, dark matter has yet to be detected directly. We thus arrive to one of the open problems in cosmology:

What is the nature of dark matter?

Since the early 2000s, we have adopted the Λ CDM model of cosmology as our standard cosmological framework. This model works on the following assumptions: The universe is flat, homogeneous, and isotropic at large scales. Around 69% of the universe is made of dark energy, here modeled as a **cosmological constant** Λ , 5% of the universe is ordinary baryonic matter, and the remaining 26% consist of **cold dark matter** (CDM).

CDM refers to dark matter that is pressureless, that is, $w_{\text{cdm}} = 0$. As a slow-moving, massive species that interacts only gravitationally, CDM provides a simple and effective mechanism for clumping and driving the formation of the large-scale structure observed in the universe today.

1.2 Moving beyond CDM: prelude to SCDM

Despite the successes of the Λ CDM model, it still faces challenges at both small and large scales. One of the most prominent issues at large scales is the **Hubble tension**, where we have a discrepancy between the inferred value of the Hubble constant H_0 from early and late-universe measurements [RCY⁺19, VTR19]. Similarly, the **S_8 tension** refers to the discrepancy in the measurement of the amplitude of matter clustering, S_8 , between weak lensing observations and the predictions of the Λ CDM model when fitted to CMB surveys. At small scales we have the too-big-to-fail [BK11], core-cusp density profile [de 10], and the too-dense-to-be-satellite problems [SL21], among others.

These challenges have inspired countless modifications to Λ CDM. In this work, we will take a different approach and question a fundamental assumption of the model:

Must $w_{\text{dm}} = 0$ in order to work?

Instead of parametrizing a $w_{\text{dm}}(a)$ curve, we focused our attention on the model of **superconducting dark matter** (SCDM), which offers underlying physical mechanisms and principles to justify the behavior of dark matter dynamically.

First introduced in a cosmological context by [TWZZ24], superconducting dark matter (SCDM) is based on the Nambu–Jona-Lasinio (NJL) model [NJL61], which itself was inspired by the Bardeen–Cooper–Schrieffer (BCS) theory of superconductivity [BCS57]. In BCS theory, there is a critical temperature below which free electrons in a conductor form Cooper pairs, lowering their energy and giving rise to superconductivity. Our work follows [LC24], where thermal corrections to SCDM were considered for the first time.

As we will show later, SCDM features an analogous transition, after which the equation of state w_{dm} , which we will now refer to as w_{scdm} , decays from 1 to $w_0 \ll 1$, its present-day value. The central question of this work is:

How large can w_0 be in this model while still matching the predictions of Λ CDM?

Chapter 2

Superconducting Dark Matter

2.1 Theory

The fermionic theory of SCDM follows:

$$\mathcal{L}_{\text{SCDM}} = \bar{\psi}(i\gamma^\mu\partial_\mu - m)\psi - \kappa\bar{\psi}\gamma^0\gamma^5\psi + \frac{(\bar{\psi}\psi)^2}{M^2} \quad (2.1)$$

Where ψ is the spin 1/2 dark matter field, $\bar{\psi} \equiv \psi^\dagger\gamma^0$ its Dirac adjoint, γ^0 is the first of four (γ^μ , $\mu = 0, 1, 2, 3$) Dirac matrices, and $\gamma^5 \equiv i\gamma^0\gamma^1\gamma^2\gamma^3$ is the ‘‘fifth’’ Dirac matrix, an operator capable of distinguishing between the left- and right-handed parts of the fermion ψ (i.e., it acts as a projection operator). Using dimensional analysis, we find that the model’s parameters κ and M have dimensions $[\kappa] = [M] = [1]$. The term $+\frac{(\bar{\psi}\psi)^2}{M^2}$ constitutes a four-fermion, scalar, attractive, self-interaction.

The $-\kappa\bar{\psi}\gamma^0\gamma^5\psi$ term doesn’t represent an interaction, at least not conventionally. It is relevant to expand the bilinear:

$$\begin{aligned} -\kappa\bar{\psi}\gamma^0\gamma^5\psi &= -\kappa\psi^\dagger\gamma^0\gamma^0\gamma^5\psi \\ &= -\kappa\psi^\dagger\gamma^5\psi \\ &= -\kappa\psi^\dagger\gamma^5(\psi_L + \psi_R) \\ &= -\kappa\psi^\dagger(-\psi_L + \psi_R) \\ &= -\kappa(\psi_L^\dagger + \psi_R^\dagger)(-\psi_L + \psi_R) \\ &= -\kappa\left(-\psi_L^\dagger\psi_L + \psi_R^\dagger\psi_R + \psi_L^\dagger\psi_R - \psi_R^\dagger\psi_L\right) \\ &= -\kappa\left(-\psi_L^\dagger\psi_L + \psi_R^\dagger\psi_R + \psi^\dagger P_L P_R \psi - \psi^\dagger P_R P_L \psi\right) \\ &= -\kappa\left(-\psi_L^\dagger\psi_L + \psi_R^\dagger\psi_R\right) \end{aligned} \quad (2.2)$$

Where P_L, P_R are the left- and right-handed projectors. The above result hints the fact that κ will quantify an energy shift and a difference in number densities between left and right handed fermions. To see this, consider reducing the model to the Dirac free lagrangian in addition to κ -term:

$$\mathcal{L}_\kappa = \bar{\psi}(i\gamma^\mu\partial_\mu - m)\psi - \kappa\bar{\psi}\gamma^0\gamma^5\psi \quad (2.3)$$

Leading to the equation of motion for ψ :

$$\begin{aligned} \frac{\partial \mathcal{L}_\kappa}{\partial \bar{\psi}} &= \partial_\mu \left(\frac{\partial \mathcal{L}_\kappa}{\partial (\partial_\mu \bar{\psi})} \right) \\ (i\gamma^\mu \partial_\mu - m)\psi - \kappa \gamma^0 \gamma^5 \psi &= 0 \\ \left(i\gamma^\mu \partial_\mu - m - \kappa \gamma^0 \gamma^5 \right) \psi &= 0 \end{aligned} \quad (2.4)$$

By assuming plane waves solutions (i.e., working in momentum space)

$$\psi(x) = u(p)e^{-ip \cdot x} \quad (2.5)$$

We observe that $\partial_\mu \rightarrow -ip_\mu$ over the solution in Eq. 2.5. As such, the expression $i\gamma^\mu \partial_\mu \rightarrow \gamma^\mu p_\mu \equiv \not{p}$. With this simplification, Eq. 2.4 becomes

$$\left(\not{p} - m - \kappa \gamma^0 \gamma^5 \right) u(p) = 0 \quad (2.6)$$

Because of commutation rules, we can project the entire equation to the left or to the right. Starting with a right-projection:

$$\begin{aligned} 0 &= \left(\not{p} - m - \kappa \gamma^0 \gamma^5 \right) P_R u(p) \\ &= \left(\not{p} - m - \kappa \gamma^0 \gamma^5 \right) u_R(p) \\ &= \left(\not{p} - m - \kappa \gamma^0 \right) u_R(p) \end{aligned} \quad (2.7)$$

The operator in parenthesis is equal to $\gamma^0(E - \kappa) - \boldsymbol{\gamma} \cdot \mathbf{p} - m$. Multiply the equation in Eq. 2.7 by $\gamma^0(E - \kappa) - \boldsymbol{\gamma} \cdot \mathbf{p} + m$. We find that six out of the nine terms vanish, and we are left with

$$\begin{aligned} 0 &= \left((E - \kappa)^2 + (\boldsymbol{\gamma} \cdot \mathbf{p})^2 - m^2 \right) u_R(p) \\ &= \left((E - \kappa)^2 - \mathbf{p}^2 - m^2 \right) u_R(p) \end{aligned} \quad (2.8)$$

Because this has to hold for any $u_R(p)$, it follows that $(E - \kappa)^2 - \mathbf{p}^2 - m^2 = 0$, in other words:

$$E_R = \sqrt{\mathbf{p}^2 + m^2} + \kappa \quad (2.9)$$

And equivalent analysis on the left-handed version of the modified Dirac equation yields

$$E_L = \sqrt{\mathbf{p}^2 + m^2} - \kappa \quad (2.10)$$

This is the first effect of the κ -term: It modifies the energies of the left- and right-handed fermions in the theory. As such, we identify κ as the **(chiral) chemical potential** of the theory.

Before moving on, it is relevant to compute the chiral number density in a \mathcal{L}_κ theory: $n_5 \equiv (n_L - \bar{n}_L) - (n_R - \bar{n}_R)$. Each term involves a Fermi-Dirac distribution:

$$f(p) = \frac{1}{1 + \exp\left(\frac{E-\mu}{T}\right)} \quad (2.11)$$

With zero total chemical potential μ (that is, the theory has an equal amount of fermions and antifermions), we don't need to worry about the subtleties of an antiparticle Fermi-Dirac distribution. Still, we should note that a right-handed antifermion's energy gets shifted by $-\kappa$ (compared to the right-handed fermion's shift of $+\kappa$). In the massless limit:

$$\begin{aligned} n_5 &= n_L - \bar{n}_L - n_R + \bar{n}_R \\ &= \int \frac{d^3p/(2\pi)^3}{e^{(p-\kappa)/T} + 1} - \int \frac{d^3p/(2\pi)^3}{e^{(p+\kappa)/T} + 1} - \int \frac{d^3p/(2\pi)^3}{e^{(p+\kappa)/T} + 1} + \int \frac{d^3p/(2\pi)^3}{e^{(p-\kappa)/T} + 1} \\ &= \frac{kT^2}{3}, \quad m = 0, \quad \kappa \ll T \end{aligned} \quad (2.12)$$

The evaluation of these integrals is a non-trivial problem. For the interested reader, a full computation with approximations can be found in Appendix A. With Eq. 2.12 in mind, we are ready to summarize the effects of the κ -term on a \mathcal{L}_κ theory (see Eq. 2.3). The effects of the $-\kappa\bar{\psi}\gamma^0\gamma^5\psi$ term include:

- Handedness-dependent energy shifts.
- Imbalance in the number of left handed and right handed particles in the universe.

From now on, it is assumed that the $\mathcal{L}_{\text{SCDM}}$ is being used in the massless ($m = 0$) case.

2.2 Scalar characterization

To study SCDM in a cosmological context, it is useful to transform the theory into a scalar theory by means of an auxiliary field, here Δ , through a Hubbard-Stratonovich transformation [Hub59, Str57]. We start by realizing the following (Euclidean path integral) identity:

$$1 = \int \mathcal{D}\Delta \exp\left(-\int d^4x \left[\frac{1}{2}M\Delta - \frac{1}{M}\bar{\psi}\psi\right]^2\right) \quad (2.13)$$

Where Δ is an auxiliary scalar field. Following the convention of [LC24], naming this field Δ makes physical sense: When the scalar field is at zero, $\Delta = 0$, we get no fermion-antifermion pairs. This is analogous to the gap energy in BCS theory.

Consider the Euclidean path integral for $\mathcal{L}_{\text{SCDM}}$:

$$\mathcal{L}_{\text{SCDM}}^E = \bar{\psi}(\gamma^\mu\partial_\mu + m)\psi + \kappa\psi\gamma^0\gamma^5\psi - \frac{(\bar{\psi}\psi)^2}{M^2} \quad (2.14)$$

$$Z_{\text{SCDM}} = \int \mathcal{D}\bar{\psi}\mathcal{D}\psi \exp\left(-\int d^4x_E \left[\bar{\psi}(\gamma^\mu\partial_\mu + m)\psi + \kappa\psi\gamma^0\gamma^5\psi - \frac{(\bar{\psi}\psi)^2}{M^2}\right]\right) \quad (2.15)$$

By inserting (Eq. 2.13) into the path integral (Eq. 2.15) of the SCDM theory, we get a Euclidean path integral over the fermionic fields and the auxiliary scalar field:

$$\begin{aligned}
Z_E &= \int \mathcal{D}\Delta \mathcal{D}\bar{\psi} \mathcal{D}\psi \exp \left(- \int d^4x_E \left[\bar{\psi}(\gamma^\mu \partial_\mu + m)\psi + \kappa \bar{\psi} \gamma^0 \gamma^5 \psi - \frac{(\bar{\psi}\psi)^2}{M^2} \right. \right. \\
&\quad \left. \left. + \left[\frac{1}{2} M \Delta - \frac{1}{M} \bar{\psi}\psi \right]^2 \right] \right) \\
&= \int \mathcal{D}\Delta \mathcal{D}\bar{\psi} \mathcal{D}\psi \exp \left(- \int d^4x_E \left[\bar{\psi}(\gamma^\mu \partial_\mu + m)\psi + \kappa \bar{\psi} \gamma^0 \gamma^5 \psi - \frac{(\bar{\psi}\psi)^2}{M^2} \right. \right. \\
&\quad \left. \left. + \frac{1}{4} M^2 \Delta^2 - \Delta \bar{\psi}\psi + \frac{1}{M^2} (\bar{\psi}\psi)^2 \right] \right) \\
&= \int \mathcal{D}\Delta \mathcal{D}\bar{\psi} \mathcal{D}\psi \exp \left(- \int d^4x_E \left[\bar{\psi}(\gamma^\mu \partial_\mu + m - \Delta - \kappa \gamma^0 \gamma^5)\psi + \frac{1}{4} M^2 \Delta^2 \right] \right)
\end{aligned} \tag{2.16}$$

This last expression tells us that we can integrate out the fermionic field using the exact functional integral/determinant:

$$\int \mathcal{D}\bar{\psi} \mathcal{D}\psi \exp \left(- \int d^4x \bar{\psi} \mathcal{G}^{-1} \psi \right) = \det(\mathcal{G}^{-1})^{-1} \tag{2.17}$$

This means that

$$Z_E = \int \mathcal{D}\Delta \exp \left(- \int d^4x_E \left[\frac{1}{4} M^2 \Delta^2 - \ln \det(\mathcal{G}^{-1}) \right] \right) \tag{2.18}$$

Where

$$\mathcal{G}^{-1} = \gamma^\mu \partial_\mu + m - \Delta - \kappa \gamma^0 \gamma^5 \tag{2.19}$$

Giving:

$$\mathcal{L}_\Delta = -\frac{1}{4} M^2 \Delta^2 + \int \frac{d^4k}{(2\pi)^4} \ln U_+ U_- \tag{2.20}$$

Where $U_\pm = \Delta^2 - \omega^2 + (k \pm \kappa)^2$, $\Delta - m \rightarrow \Delta$, and $\mathcal{G}^{-1} = -\gamma^\mu k_\mu + \Delta - m - \kappa \gamma^0 \gamma^5$ in momentum space. To leading order, the computation of the energy-momentum integral leads to the effective potential [LC24]:

$$V_{\text{eff}}(\Delta) = \frac{1}{4} M^2 (\Delta + m)^2 + \frac{\Delta^4}{32\pi^2} \left(1 + 4 \ln \frac{\Delta}{\Lambda_{\text{UV}}} \right) - \frac{\kappa^2 \Delta^2}{4\pi^2} \left(1 - 2 \ln \frac{\Delta}{\Lambda_{\text{UV}}} \right) + V_0 \tag{2.21}$$

Where the model parameters must follow the hierarchy

$$M \gtrsim \Lambda_{\text{UV}} \gtrsim \kappa \tag{2.22}$$

for self-consistency [LC24]. When the parameters are much larger than the local values of Δ (an assumption that will happen, as we will work with families of parameters where $M, \Lambda_{\text{UV}}, \kappa$ are of order TeV and Δ is of order eV), the minimum of the potential can be approximated by

$$\Delta_0 \approx \Lambda_{\text{UV}} \exp \left(-\frac{\pi^2}{2} \left(\frac{M}{\kappa} \right)^2 \right). \tag{2.23}$$

The role of V_0 in the potential (Eq. 2.21) is to produce a lift that, although it won't make a difference from a particle physics point of view, it will avoid SCDM from becoming dark energy in a cosmological context.

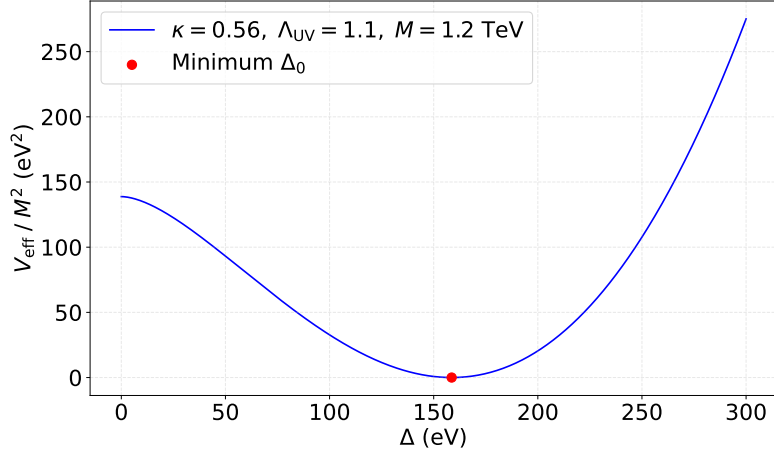


Figure 2.1: Scalar effective potential. Plot of the scalar effective potential in Eq. 2.21. The approximation to the location of the minimum, Eq. 2.23, has an error of $2.261 \times 10^{-6}\%$ compared to a numerically-found minimum location.

A fermionic thermal correction can be computed for the theory. The Euclidean four-momentum $k^\mu = (\omega, \mathbf{k})$ gets promoted with Matsubara modes of the fermionic kind: $\omega \rightarrow \omega_n = \frac{\pi(2n+1)}{\beta} = T\pi(2n+1)$. With the energy integral becoming an infinite sum over the discrete modes, the thermal one loop correction follows:

$$\mathcal{L}_{\text{thermal}}^{\text{1-loop}} = \int \frac{d^3k}{(2\pi)^3} T \sum_{n=-\infty}^{\infty} \ln \frac{1}{T^4} U_{n+} U_{n-} \quad (2.24)$$

Where $U_{n\pm} = \Delta^2 + \omega_n^2 + (k \pm \kappa)^2$, and T stands for the temperature of the dark sector. This gives an effective thermal potential contribution of [LC24]:

$$V_{\text{thermal}}^{\text{1-loop}} = -\frac{2T^4}{\pi^2} \left(I_2(\Delta/T) + \frac{\kappa^2}{T^2} I_0(\Delta/T) \right) \quad (2.25)$$

Where I_0, I_2 are instances of thermal integrals:

$$I_n(x) = \int_0^\infty ds s^n \ln(1 + \exp(-\sqrt{s^2 + x^2})). \quad (2.26)$$

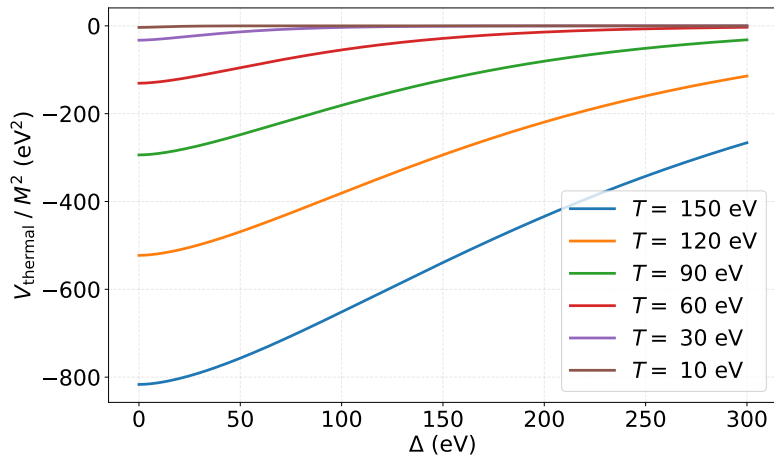


Figure 2.2: 1-loop thermal corrections. Plots of the 1-loop thermal correction as given in Eq. 2.25 for various temperatures with $\kappa = 0.56$ TeV.

For $x \neq 0$, the thermal integrals in Eq. 2.26 must be evaluated numerically. Figure 2.3 shows the shape of the total potential (effective plus 1-loop thermal corrections) at different temperatures. Note that the thermal corrections will push the location of the total potential (zero temperature effective plus thermal correction) towards $\Delta = 0$. It is not until the temperature drops enough for the thermal correction to be negligible compared to the effective potential that the approximation in Eq. 2.23 becomes valid.

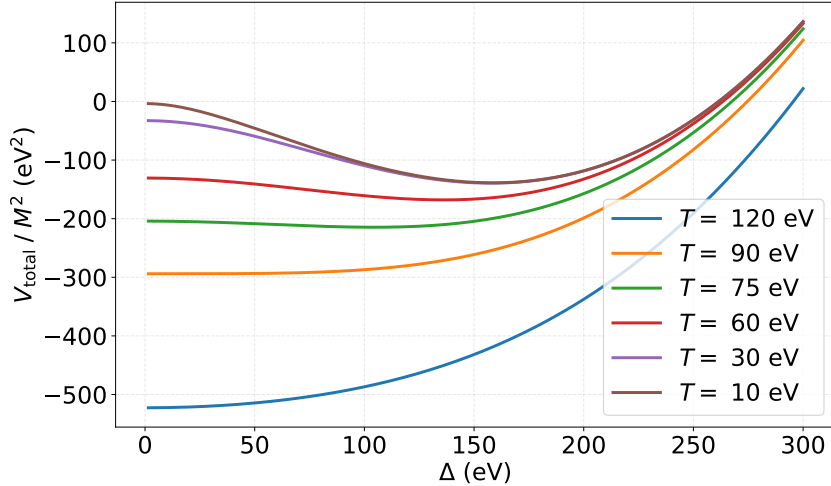


Figure 2.3: Total potential. Plots of $V_{\text{total}} = V_{\text{eff}} + V_{\text{thermal}}^{1\text{-loop}}$ at various temperatures. For these plots, $\kappa = 0.56$ TeV, $M = 1.2$ TeV, $\Lambda_{\text{UV}} = 1.1$ TeV.

As the temperature of the dark sector drops, there will be a critical temperature T_C at which the potential minimum no longer occurs at $\Delta = 0$. This corresponds to a 2nd order phase transition in the model, as the minimum shifts away from the origin in a smooth, continuous manner.

To find the critical temperature, we identify that the problem has an associated gap equation

$$\frac{\partial V}{\partial \Delta} = 0 \quad (2.27)$$

With boundary condition

$$\Delta(T = T_C) = 0 \quad (2.28)$$

Where we note that this analysis takes T as a quantity that increases. In other words, T_C is the temperature at which $\Delta = 0$ as we heat up the dark sector. By assuming a small x in $I_n(x)$, one can approximate the solution to the gap equation [LC24] with:

$$T_C = \Delta_0 \frac{\exp(\gamma_e)}{\pi} \quad (2.29)$$

Where $\gamma_e \approx 0.577216$ is the Euler-Mascheroni constant.

2.3 Cosmological Evolution

To derive the thermal evolution of the model, we employ the following characterizations of pressure and energy density:

$$p = -V \quad (2.30)$$

$$\rho = T \frac{dp}{dT} - p \quad (2.31)$$

Where Eq. 2.30 comes from taking the static limit in the classical field definition of pressure:

$$p = \frac{1}{2}(\dot{\Delta})^2 - V(\Delta) \quad (2.32)$$

And Eq. 2.31 can be derived from the equations of energy density and pressure in momentum space [Dod03]:

$$\rho = g \int \frac{d^3p}{(2\pi)^2} E(p) f(x, p) \quad (2.33)$$

$$P = g \int \frac{d^3p}{(2\pi)^3} \frac{p^2}{3E(p)} f(x, p) \quad (2.34)$$

Where g quantifies the number of internal degrees of freedom and f is the distribution function for the species. To go from these two equations to Eq. 2.31, we need to assume that the distribution functions depend only on E/T . We will further take the massless limit. Observing that

$$E(p) = \sqrt{p^2 + m^2} \rightarrow p \quad (2.35)$$

We perform a change of variables into $q = p/T$. Then

$$E(q) = Tq, \quad (2.36)$$

and the differential transforms as:

$$d^3p = T^3 d^3q. \quad (2.37)$$

In terms of q , we see that ρ, P take the forms:

$$\rho = g \int \frac{d^3q}{(2\pi)^2} T^4 q f(q) \quad (2.38)$$

$$P = g \int \frac{d^3q}{(2\pi)^3} T^4 \frac{q}{3} f(q) \quad (2.39)$$

From which we immediately conclude that

$$\rho = 3P, \quad (2.40)$$

and that P as given in Eq. 2.39 satisfies:

$$\begin{aligned} \frac{dP}{dT} &= 4g \int \frac{d^3q}{(2\pi)^3} T^3 \frac{q}{3} f(q) \\ &= \frac{4}{T} P. \end{aligned} \quad (2.41)$$

By noting that $4P = 3P + P = \rho + P$, we conclude that 2.41 is equivalent to 2.31.

At early times, before the phase transition ($T > T_C$), $\Delta = 0$ statically, as the minimum of the total potential stays at the origin at these temperatures (hence the aforementioned approximation $\dot{\Delta} = 0$). As such, the effective potential will have no contribution to p_Δ , and the thermal integrals will have an exact analytic solution, yielding:

$$\begin{aligned} p_\Delta &= \frac{2T^4}{\pi^2} \left(I_2(0) + \frac{\kappa^2}{T^2} I_0(0) \right) \\ &= \frac{2T^4}{\pi^2} \left(\frac{7\pi^4}{360} + \frac{\kappa^2}{T^2} \frac{\pi^2}{12} \right) \\ &= \frac{7\pi^2 T^4}{180} + \frac{T^2 \kappa^2}{6} \end{aligned} \quad (2.42)$$

The energy density ρ_Δ follows from it:

$$\begin{aligned} \rho_\Delta &= T \frac{dp_\Delta}{dT} - p_\Delta \\ &= T \frac{d}{dT} \left(\frac{7\pi^2 T^4}{180} + \frac{T^2 \kappa^2}{6} \right) - \frac{7\pi^2 T^4}{180} - \frac{T^2 \kappa^2}{6} \\ &= \frac{7\pi^2 T^4}{60} + \frac{T^2 \kappa^2}{6} \end{aligned} \quad (2.43)$$

By computing the equation of state w_Δ :

$$\begin{aligned} w_\Delta &= \frac{p_\Delta}{\rho_\Delta} \\ &= \frac{7\pi^2 T^2 + 30\kappa^2}{21\pi^2 T^2 + 30\kappa^2} \end{aligned} \quad (2.44)$$

We observe that w_Δ has 2 characteristic values. At high T , in particular $T \gg \kappa$, $w_\Delta \sim \frac{7\pi^2 T^2}{21\pi^2 T^2} = 1/3$. Once the dark sector cools down and $T \lesssim \kappa$, the other terms dominate and $w_\Delta \sim \frac{30\kappa^2}{30\kappa^2} = 1$. This transition is plotted on Fig. 2.5.

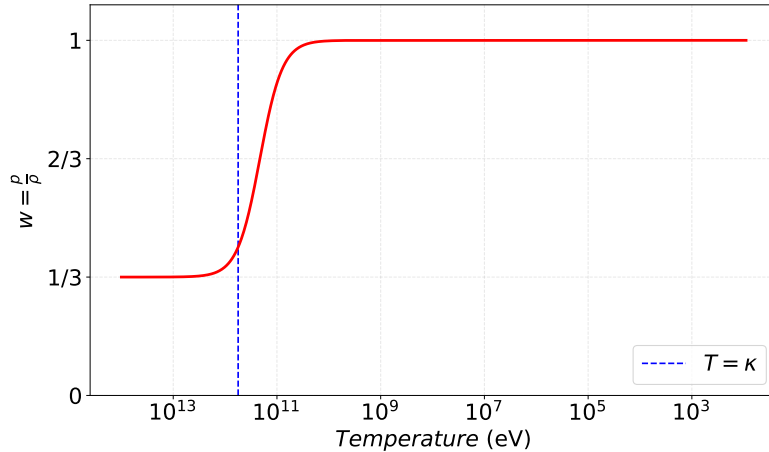


Figure 2.4: Evolution of the equation of state w_Δ at early times.

By assuming that the dark sector was in thermal equilibrium with the standard model (SM) at early times, as well as adiabaticity in the thermal evolution:

$$s = \frac{\rho_\Delta + p_\Delta}{T_\Delta} \propto (z + 1)^3, \quad (2.45)$$

we find that

$$T(z+1) = \frac{\sqrt[3]{5} \left(\sqrt[3]{2} \left(\sqrt{7} \sqrt{567\pi^2 C^2 (z+1)^6 + 20\kappa^6} + 63\pi C (z+1)^3 \right)^{2/3} - 2\sqrt[3]{35\kappa^2} \right)}{14^{2/3} \pi \sqrt[3]{\sqrt{7} \sqrt{567\pi^2 C^2 (z+1)^6 + 20\kappa^6} + 63\pi C (z+1)^3}} \quad (2.46)$$

Where C is a constant of proportionality to be found by equating the temperature of the SM at early times with the that of the standard model. In particular:

$$C = \frac{1}{(1+z)^3} \left(\frac{7}{45} \pi^2 T^3 + \frac{1}{3} T \kappa^2 \right) \quad (2.47)$$

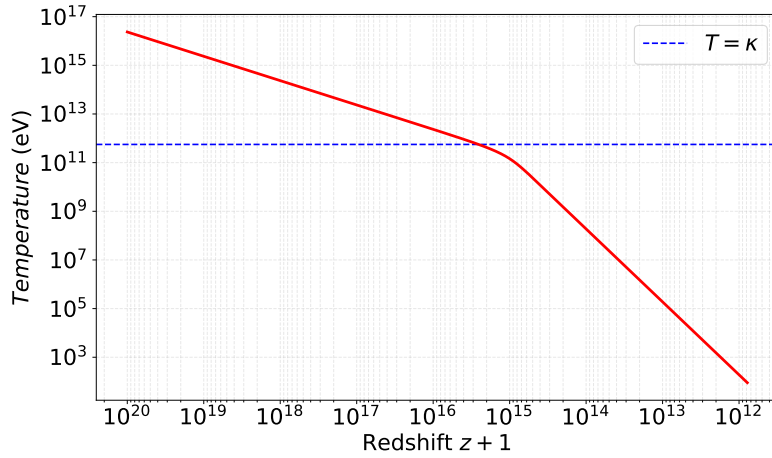


Figure 2.5: Redshift dependence on the temperature of the dark sector.

Plot of Eq. 2.46 with C computed using the temperature of the SM at redshift $z+1 = 10^{20}$ ($\sim 2.34822 \times 10^{16}$ eV). Increasing the SM matching temperature has negligible effects on the figure. Observe that at high redshift ($T > \kappa$), $T \propto Z$ as expected from a particle with $w = 1/3$. Once $T < \kappa$, $T \propto Z^3$, which is expected from a particle with $w = 1$.

Once T_Δ drops to T_C , equation 2.44 stops being valid as Δ starts rolling away from the origin. As the second order phase transition occurs, the evolution of w_Δ to today's value is approximately given by [LC24]

$$(1+z)^3 \sim \frac{w_0(1+w_\Delta)}{w_\Delta(1+w_0)} \exp\left(\frac{1}{w_0} - \frac{1}{w_\Delta}\right) \quad (2.48)$$

Where w_0 is the value of w_Δ today.

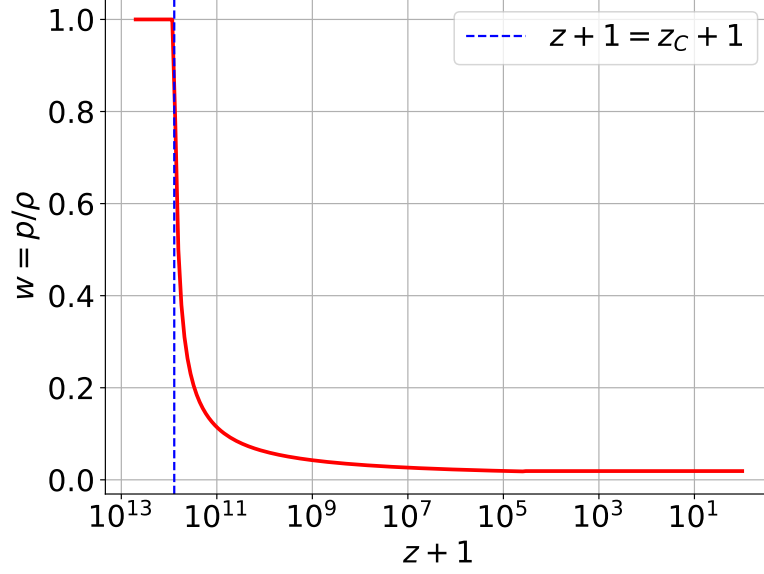


Figure 2.6: Equation of state w_Δ at late times. Plot of Eq. 2.48 with $w_0 = 0.0115038$, the corresponding value for a model with $\kappa = 0.56$ TeV, $M = 1.2$ TeV, and $\Lambda_{\text{UV}} = 1.1$ TeV.

Although there is a one-to-one relation between the critical redshift $(1+z)_C$ and w_0 , if we want to compute κ for a given curve of the form 2.48, and needs to set a value for T_C (or vice versa, set a value of κ and find T_C).

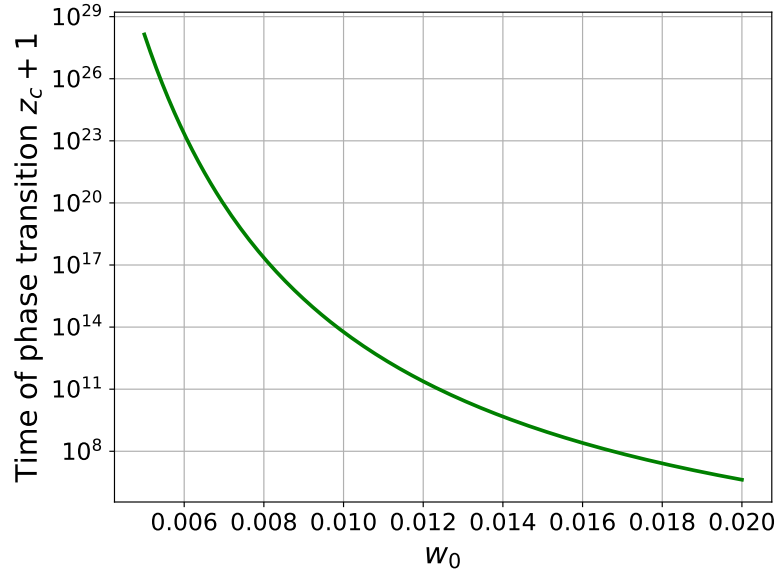


Figure 2.7: Relation between w_0 and the time of phase transition, $z_c + 1$.

Chapter 3

Cosmological Impacts of SCDM

3.1 CLASS and Its Modifications

Equation 2.48 quantifies the evolution of a massless SCDM theory at the cosmological level, as any impacts on the evolution of cosmological perturbations depend on the value of w_Δ at any time.

To investigate how a universe dominated by superconducting dark matter would differ from one governed by cold dark matter, we employed the Cosmic Linear Anisotropy Solving System (CLASS) code [Les11, BLT11]. CLASS is a Boltzmann solver capable of modeling cosmological background evolution and perturbations. The rest of this section will describe, in detail, how SCDM was implemented to work within the CLASS code.

The already existing CLASS particle species `background_fluid` (background fluid) works by, superficially, specifying the value of $w(a)$ and $\frac{dw}{da}$ at any time in the time domain of the simulation.

Given that equation 2.48 defines an implicit dependence between w and z , solving for w requires numerical *root-finding* methods. This can be computationally intensive over multiple values of z (equivalently, scale factor values a). To improve the workflow of CLASS, we precomputed $w(a)$ for different values of w_0 in the time domain bounded below by $a = 10^{-14}$:

$$10^{-14} \leq a \leq 1 \quad \Leftrightarrow \quad 10^{14} \geq z + 1 \geq 1. \quad (3.1)$$

The `root` method of `scipy` [VGS20] is able to solve for w with high precision. It is worth noting it requires a close initial guess in order to work. We recommend updating the initial guess to w_0 every time the value of w_0 is changed.

The code implementing this solver is shown in Appendix B. This code outputs data sets in the way our modified CLASS code needs them. A total of four data files are exported:

1. Scale factor values.

A single-column csv file is exported containing the discretized scale factor values used to compute the remaining three data sets. Note that this is the corresponding data set used to interpolate in SCDM CLASS code.

2. $w(a)$ values.

Given a smallest and largest w_0 values, the python code will create a linear space of w_0 values within them. For each value of w_0 (here representing a column in the dataset), the implicit equation 2.48 is solved for w for scale factor values in the domain.

3. $w'(a) \equiv \frac{dw}{da}$ values.

Although there is no explicit equation relating w to a , one can compute an implicit integral and use the value found in the previous step to exactly compute $\frac{dw}{da}$ at any value of a .

$$\frac{dw}{da} = \frac{-3w^2(1+w)}{a} \quad (3.2)$$

4. Continuity equation integrals.

Due to the lack of explicit parametric descriptions for $w(a)$, we decided to precompute integrals of the form

$$\int_{a_i}^1 \frac{3(1+w)}{a} da \quad (3.3)$$

For $a_i \in [10^{-14}, 1]$. These integral comes from solving the continuity equation, and CLASS uses the values in this data set to compute the evolution of ρ_{scdm} , for example.

We note that `scipy`'s `quad` numerical method suffices, with increasing precision and velocity when recasting the integral to one in terms of $d(\ln a)$. An essential improvement when computing this integral comes in the form of interpolators. The precomputed $w(a)$ data can be used to define interpolators and avoid solving for the roots of Eq. 2.48.

CLASS processes the four datasets before starting background cosmological computations. A value of w_0 is supplied in the standard `.ini` file along with the rest of the family of cosmological parameters. Based on the supplied value of w_0 , CLASS finds the best suitable pair of neighboring columns in the datasets to create a new triplet of one dimensional data sets that best match the supplied w_0 . The two neighboring columns are weighted through linear interpolation.

Once CLASS interpolates the data sets to create w_0 -specific data, it continues running as in the original code. Beyond this data processing procedures, the original CLASS code differs to our modified SCDM CLASS code in that the `background_w fld()` function within `background.c`, where the information for the fluid is computed, now works using interpolators making use of the previously generated data arrays. Data arrays are interpolated using the CLASS function `array_interpolate_linear`. This function was adequate for two reasons:

1. Linear interpolation is sufficient for the current problem.
2. It keeps track of the previously used interpolation index, accelerating substantially the process of interpolation.

An ideal SCDM computation would use that $\Omega_{\text{cdm}} = 0$ (that is, a universe with no cold dark matter). Still, due to the manner in which CLASS handles the cosmological synchronous gauge, a small amount of CDM must be present. In the following sections, any SCDM computation was carried out in a universe with $\Omega_{\text{cdm}} = 10^{-10}$.

To compare the observables in a SCDM universe with that of a CDM universe in a sensible manner, we assume that $\rho_{\text{scdm}} = \rho_{\text{cdm}}$ today. In practice, we achieve this by setting $\Omega_{\text{scdm},0}$, the density parameter for SCDM today, to a value larger than that of Ω_{cdm} in its respective case. In particular,

$$\Omega_{\text{scdm},0} = 0.267395, \quad (3.4)$$

a value that is 0.893% larger than the one used for CDM universes. As little as w_0 can be, the fact that it is nonzero drastically changes the way the universe behaves throughout its evolution.

The last assumption we make is that SCDM simulations are computed using a larger value of `N_ur` (the effective number of relativistic species) compared to the CDM universe value of 3.044. The new value is set by the condition that matter-radiation equality occurs at $z_{\text{eq}} \sim 3405.75$. We note that SCDM universes using `N_ur`=3.044 observe, in general, an earlier matter-radiation equality time. Figure 3.1 shows the relation between the size of w_0 and the required `N_ur`.

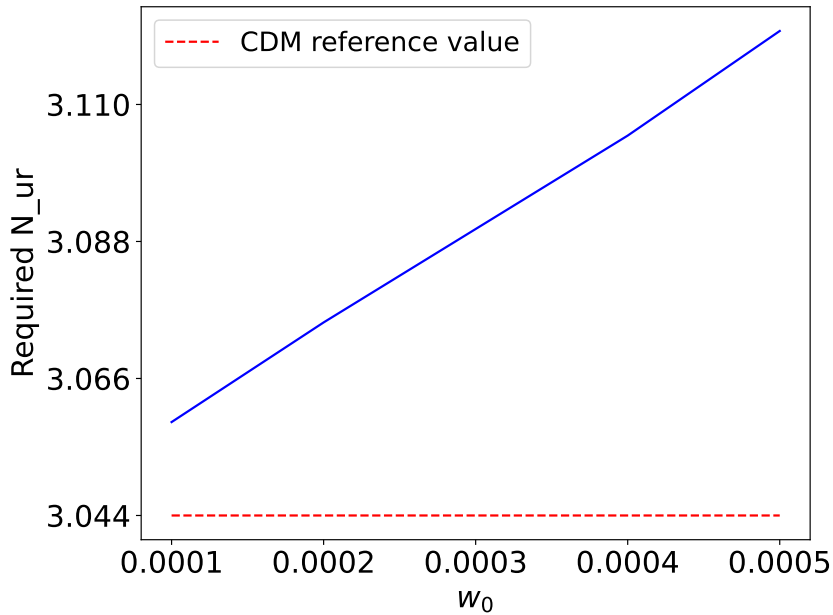


Figure 3.1: Required `N_ur` at different values of w_0 . The larger w_0 is, the larger `N_ur` needs to be in order to get $z_{\text{eq}} \sim 3405.75$ in a SCDM simulation.

By having simulations at equal z_{eq} times, we are able to properly compare observables such as the matter power spectrum and CMB spectra between SCDM and CDM universes. CDM observables and quantities are computed with a standard Λ CDM universe using Planck’s 2018 best fit parameters [Pla20b] parameters. SCDM simulations share the same parameters, except for the aforementioned modification to Ω_{cdm} and `N_ur`.

3.2 Background Quantities

The first effects of SCDM in the universe can be understood by studying the evolution of its energy density, ρ_{scdm} . Imposing the condition $\rho_{\text{cdm}} = \rho_{\text{scdm}}$ today, the faster dilution of SCDM energy density implies that $\rho_{\text{scdm}} > \rho_{\text{cdm}}$ at earlier times. This behavior is illustrated in Fig. 3.2.

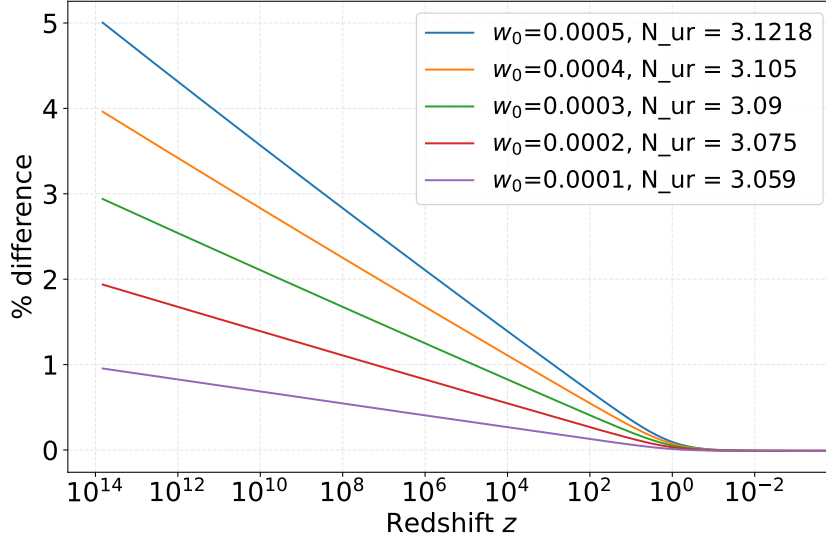


Figure 3.2: Percentage difference in the evolution of the energy density of dark matter. SCDM energy density is compared to CDM energy density for different values of w_0 . The CDM energy density was computed in a standard Λ CDM universe.

Since SCDM has a higher energy density in the past, the Hubble rate (H) in an SCDM universe is expected to be higher than in a CDM universe at all times. The percentage differences for $H(z)$ in a SCDM universe and a CDM universe is shown in figure 3.3.

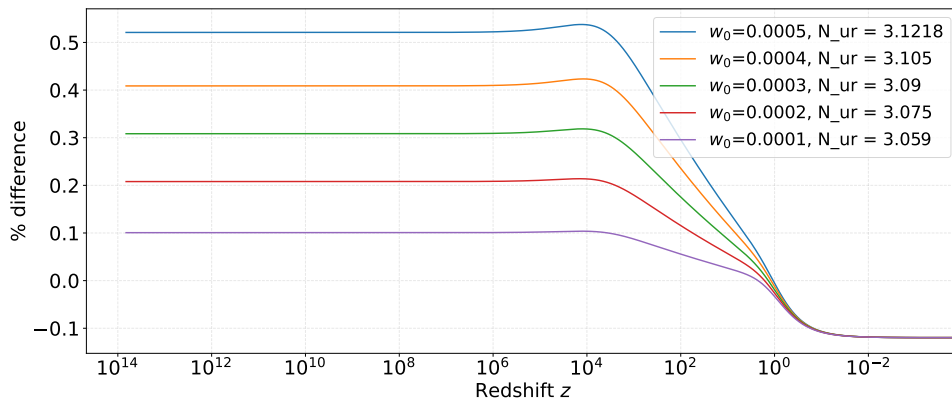


Figure 3.3: Percentage difference in the evolution of the Hubble rate between a universe with SCDM and one with CDM. The Hubble rate of SCDM dominated universes is compared to the Hubble rate in a CDM dominated universe. The CDM Hubble rate was computed in a standard Λ CDM universe.

As expected, a larger energy density ρ_{scdm} yielded a larger Hubble rate at early times for the selected values of w_0 . Still, we observe that at late times SCDM universes have a smaller Hubble rate than the reference CDM universe. This is one of the characteristic features of SCDM.

3.3 Matter Power Spectrum

Figure 3.4 compares the matter power spectrum of an SCDM universe with that of a CDM universe, using parameters from Planck 2018's best fit. At large scales (k smaller than 10^{-3} , or scales larger than ~ 6000 Mpc), the SCDM model predicts $\sim 0.15\%$ more structure, with little sensitivity to the value of w_0 .

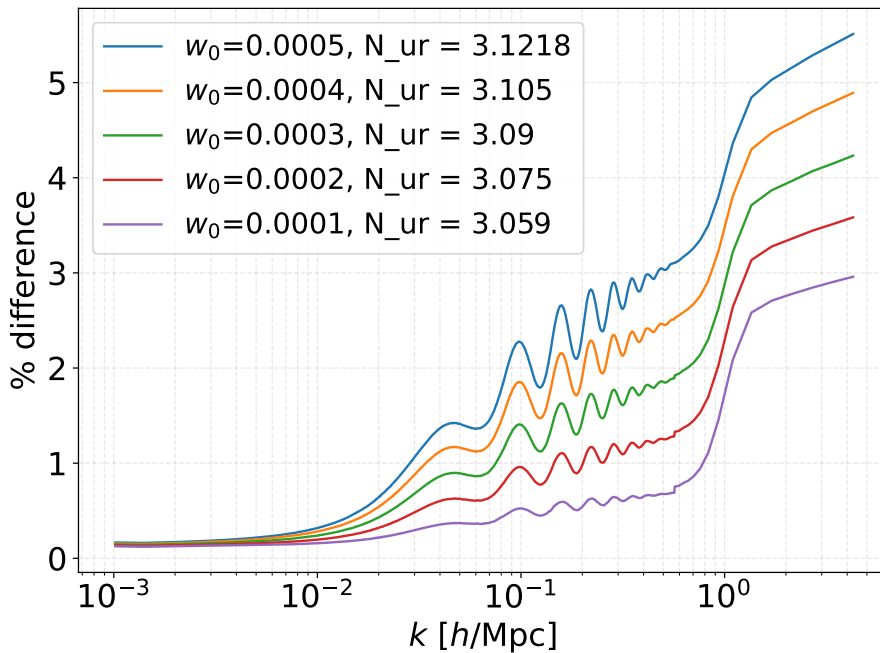


Figure 3.4: Percentage difference in the Matter Power Spectrum between a universe with SCDM and one with CDM. The matter power spectrum today ($z = 0$) in SCDM dominated universes is compared to the matter power spectrum in a CDM dominated universe.

At smaller scales ($k > 10^{-3}$), the predicted increase in structure is significantly more sensitive to the value of w_0 .

3.4 Impacts on the CMB

The effects of SCDM on the CMB are shown in Figure 3.5. Overall, SCDM consistently predicts greater Temperature-Temperature anisotropies than CDM. Additionally, regardless of the value of w_0 , SCDM tends to predict enhanced anisotropy at certain multipole moments ℓ , while at other ℓ values, it predicts slightly suppressed anisotropy — though still greater than that predicted by CDM.

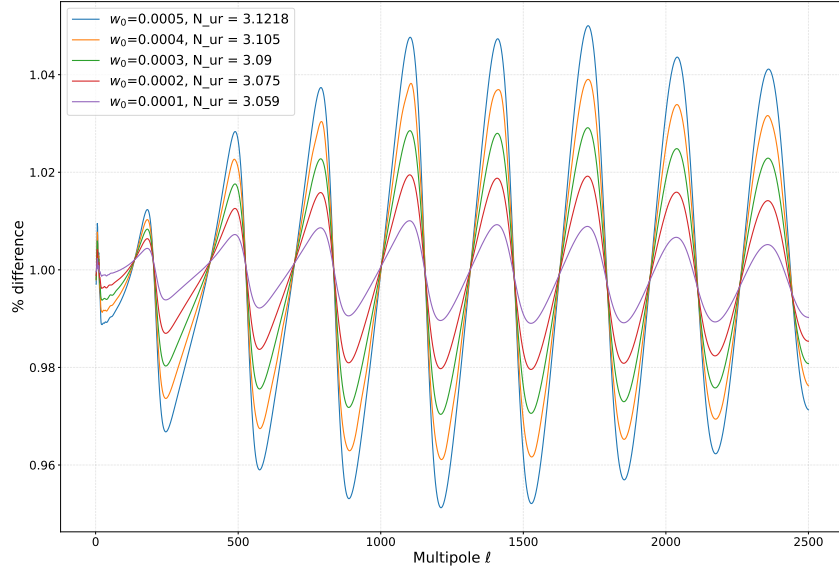


Figure 3.5: Percentage difference in the TT CMB anisotropy spectrum between a universe with SCDM and one with CDM.

Figure 3.7 shows the TT anisotropy spectra for SCDM residuals compared to the binned Planck 2018 data [Pla20a]. Visually, the SCDM curves fall within the Planck error bars to a similar degree as the best-fit CDM curve: sometimes passing through the error bars, sometimes not. Similarly, SCDM gets closer to the observations compared to CDM at certain multiple values, and vice versa. At this stage, we do have no measurement of the agreement, but the overall visual consistency, compared to a CDM universe, is comparable.

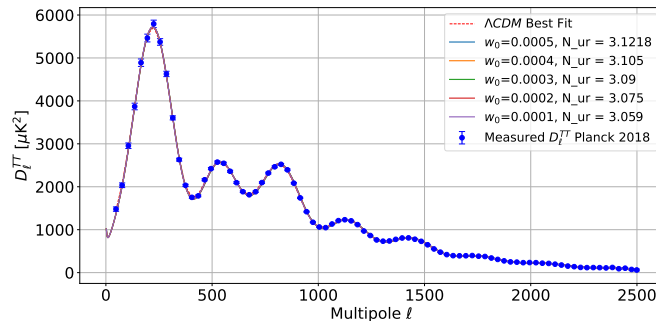


Figure 3.6: TT CMB anisotropy spectrum for SCDM universes, the best-fit Λ CDM universe, and the observations from Planck 2018.

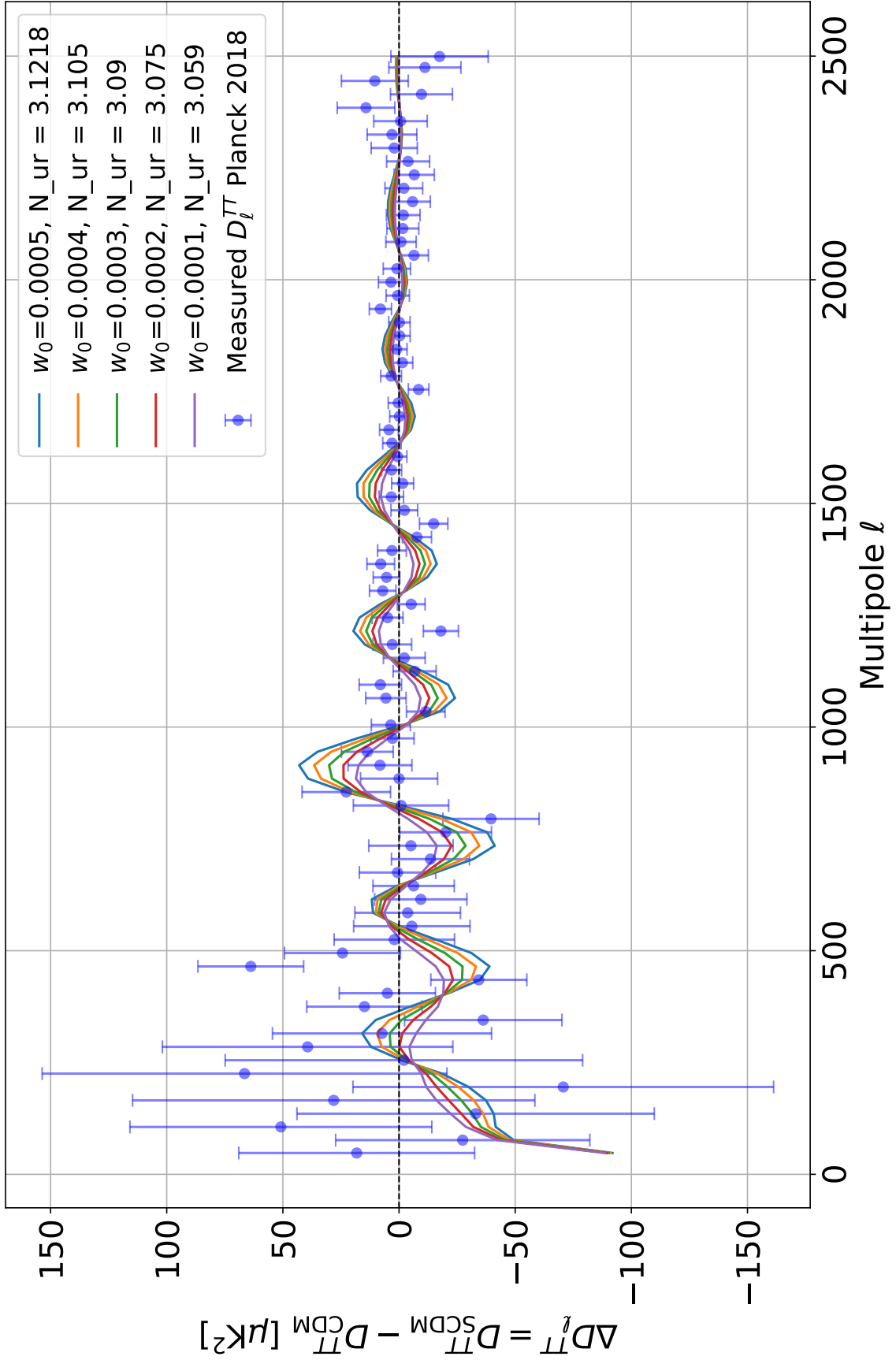


Figure 3.7: Residual comparison between SCDM universes and observations, in relation to the best-fit Λ CDM universe.

Chapter 4

Conclusion and Future Work

Superconducting Dark Matter (SCDM) provides a physically motivated framework to question the assumption that $w_{\text{dm}} = 0$ in a conservative manner, allowing for a small but nonzero range, $0 < w_{\text{scdm}} < 0.1$. This approach is advantageous compared to studies that impose a dark matter equation of state without invoking or developing an underlying physical theory.

After reviewing the field theory of SCDM, we derived the equations governing its evolution and cosmological behavior. A distinguishing feature of this model is that, although w remains small, it is not constant, instead decaying dynamically to its present-day value, w_0 .

This time-dependent behavior leads to a rich evolution of the SCDM energy density, ρ_{scdm} . We confirmed this evolution by modeling a universe dominated by SCDM in the Cosmic Linear Anisotropy Solving System (CLASS). Our predictions for the evolution of the Hubble parameter were also validated through these initial computational experiments.

After computing the matter power spectra and CMB TT anisotropy spectra for SCDM universes, we observed that SCDM consistently predicts more matter structure as well as temperature anisotropies. A first pass analysis to compare Planck 2018 data with the SCDM model showed that w_0 can stay relatively away from 0 and still fall within acceptable bounds.

Therefore, we conclude that relaxing the assumption that dark matter must satisfy $w_{\text{dm}} = 0$ at all times is a viable approach. This perspective opens the door to proposing novel models, such as SCDM, aimed at probing the fundamental nature of dark matter.

Our next step will involve running Monte Carlo Markov Chain (MCMC) analyses to quantify the degree of compatibility between the model and observations of our universe, as well as to determine the most favorable value of w_0 .

Thus far, our analysis has been bounded below by a time scale of $a = 10^{-14}$, meaning that the early evolution of the model we derived is not captured in our simulations when w_0 is very small. This limitation raises two questions: How would our current predictions change if the $w_{\text{scdm}} = 1 \rightarrow w \ll 1$ phase transition occurred within this window? And what impact might the model have on the very early universe?

Bibliography

- [Bau22] Daniel Baumann. *Cosmology*. Cambridge University Press, 2022.
- [BCS57] J. Bardeen, L. N. Cooper, and J. R. Schrieffer. Theory of superconductivity. *Phys. Rev.*, 108:1175–1204, Dec 1957.
- [BK11] Michael et al. Boylan-Kolchin. Too big to fail? the puzzling darkness of massive milky way subhaloes. *Monthly Notices of the Royal Astronomical Society: Letters*, 415(1):L40–L44, 07 2011.
- [BLT11] Diego Blas, Julien Lesgourgues, and Thomas Tram. The cosmic linear anisotropy solving system (class). part ii: Approximation schemes. *Journal of Cosmology and Astroparticle Physics*, 2011(07):034–034, July 2011.
- [Clo06] Douglas et al. Clowe. A Direct Empirical Proof of the Existence of Dark Matter. *The Astrophysical Journal*, 648(2):L109–L113, September 2006.
- [COB92] COBE Collaboration. Structure in the coBE differential microwave radiometer first-year maps. *The Astrophysical Journal Letters*, 396:L1–L5, 1992.
- [de 10] W.J.G. de Blok. The Core-Cusp Problem. *Advances in Astronomy*, 2010:789293, January 2010.
- [Dod03] Scott Dodelson. *Modern Cosmology*. Academic Press, Amsterdam, 2003.
- [Hub29] Edwin Hubble. A relation between distance and radial velocity among extragalactic nebulae. *Proc. Nat. Acad. Sci.*, 15:168–173, 1929.
- [Hub59] J. Hubbard. Calculation of partition functions. *Phys. Rev. Lett.*, 3:77–78, Jul 1959.
- [LC24] Guanming Liang and Robert R. Caldwell. Cold dark matter based on an analogy with superconductivity, 2024.
- [Les11] Julien Lesgourgues. The cosmic linear anisotropy solving system (class) i: Overview. 2011.
- [NJJ61] Y. Nambu and G. Jona-Lasinio. Dynamical model of elementary particles based on an analogy with superconductivity. i. *Phys. Rev.*, 122:345–358, Apr 1961.
- [Pla14] Planck Collaboration. Planck 2013 results. i. overview of products and scientific results. *Astronomy & Astrophysics*, 571:A1, 2014.

- [Pla20a] Planck Collaboration. Planck 2018 results. i. overview and the cosmological legacy of planck. *Astronomy & Astrophysics*, 641:A1, 2020.
- [Pla20b] Planck Collaboration. Planck 2018 results. VI. Cosmological parameters. *Astronomy & Astrophysics*, 641:A6, September 2020.
- [RCY⁺19] Adam G. Riess, Stefano Casertano, Wenlong Yuan, Lucas M. Macri, and Dan Scolnic. Large magellanic cloud cepheid standards provide a 1 *The Astrophysical Journal*, 876(1):85, May 2019.
- [Rub80] V. C. et al. Rubin. Rotational properties of 21 SC galaxies with a large range of luminosities and radii, from NGC 4605 (R=4kpc) to UGC 2885 (R=122kpc). *Astrophysical Journal*, 238:471–487, June 1980.
- [SL21] Mohammadtaher Safarzadeh and Abraham Loeb. A new challenge for dark matter models, 2021.
- [Str57] R.L. Stratonovich. On a Method of Calculating Quantum Distribution Functions. *Soviet Physics Doklady*, 2:416, July 1957.
- [TS04] Max Tegmark and Michael A. et al. Strauss. Cosmological parameters from SDSS and WMAP. *Physical Review D*, 69(10):103501, May 2004.
- [TWZZ24] Xi Tong, Yi Wang, Chen Zhang, and Yuhang Zhu. Bcs in the sky: signatures of inflationary fermion condensation. *Journal of Cosmology and Astroparticle Physics*, 2024(04):022, April 2024.
- [VGS20] Pauli Virtanen, Ralf Gommers, and SciPy 1.0 Contributors. SciPy 1.0: Fundamental Algorithms for Scientific Computing in Python. *Nature Methods*, 17:261–272, 2020.
- [VTR19] Licia Verde, Tommaso Treu, and Adam G. Riess. Tensions between the early and late Universe. *Nature Astronomy*, 3:891–895, September 2019.
- [Wei08] Steven Weinberg. *Cosmology*. 2008.
- [WMA03] WMAP Collaboration. First-year wilkinson microwave anisotropy probe (wmap) observations: Preliminary maps and basic results. *The Astrophysical Journal Supplement Series*, 148(1):1–27, 2003.
- [Zwi37] F. Zwicky. On the Masses of Nebulae and of Clusters of Nebulae. *Astrophysical Journal*, 86:217, October 1937.

Appendix A: Evaluation of Fermi-Dirac integrals

$$\begin{aligned}
n_5 &= n_L - \bar{n}_L - n_R + \bar{n}_R \\
&= \int \frac{d^3p/(2\pi)^3}{e^{(p-\kappa)/T} + 1} - \int \frac{d^3p/(2\pi)^3}{e^{(p+\kappa)/T} + 1} - \int \frac{d^3p/(2\pi)^3}{e^{(p+\kappa)/T} + 1} + \int \frac{d^3p/(2\pi)^3}{e^{(p-\kappa)/T} + 1} \\
&= \int \frac{p^2 dp/2\pi^2}{e^{(p-\kappa)/T} + 1} - \int \frac{p^2 dp/2\pi^2}{e^{(p+\kappa)/T} + 1} - \int \frac{p^2 dp/2\pi^2}{e^{(p+\kappa)/T} + 1} + \int \frac{p^2 dp/2\pi^2}{e^{(p-\kappa)/T} + 1} \\
&= \frac{1}{\pi^2} \int \frac{p^2 dp}{e^{(p-\kappa)/T} + 1} - \frac{1}{\pi^2} \int \frac{p^2 dp}{e^{(p+\kappa)/T} + 1}
\end{aligned}$$

Let $u = p/T$ and $r = \kappa/T$. Then

$$\begin{aligned}
&= \frac{1}{\pi^2} \int \frac{T^2 u^2 T du}{e^{u+r} + 1} - \frac{1}{\pi^2} \int \frac{T^2 u^2 T du}{e^{u-r} + 1} \\
&= \frac{T^3}{\pi^2} \int \frac{u^2}{e^{u+r} + 1} - \frac{u^2}{e^{u-r} + 1} du
\end{aligned}$$

To simplify the integrand, we can perform a linear approximation on the denominators. Let

$$f(u) = \frac{1}{e^u + 1}$$

Then

$$\begin{aligned}
\frac{1}{e^{u\pm r} + 1} &\approx f(u) \pm r f'(u) \\
&= \frac{1 \mp e^u (r \mp 1)}{(1 + e^u)^2}
\end{aligned}$$

Therefore the integrand can be approximated by:

$$\frac{u^2}{e^{u-r} + 1} - \frac{u^2}{e^{u+r} + 1} \approx u^2 \left(2r \frac{e^u}{(1 + e^u)^2} \right)$$

So

$$\begin{aligned}
n_5 &= \frac{2rT^3}{\pi^2} \int_0^\infty \frac{u^2 e^u}{(1 + e^u)^2} du \\
&= \frac{2T^3}{\pi^2} \frac{\kappa}{T} \cdot \frac{\pi^2}{6} \\
&= \boxed{\frac{T^2 \kappa}{3}}
\end{aligned}$$

Where $\int_0^\infty \frac{u^2 e^u}{(1+e^u)^2} du$ is a computable integral by many standard software. An analytic solution without additional assistance would identify the connection between the integral and integrals of the form $\int_0^\infty x e^{-nx} dx$ for $n \in \mathbb{Z}^+$.


```

36 # of sig. figs. in the above rounding procedure. Otherwise the data
    will look like
37 # A step/staircase function!
38
39 # Integral with respect to d(log(a))
40 def integrate_function_interpolatedlog(f,lower_bound, interp):
41     IntegralResult, IntegralError = quad(lambda x: f(x, interp), np.log
    (lower_bound), 0)
42     return IntegralResult
43
44 # Integrand in log(a) form
45 def function_to_integrate_interpolatedlog(loga,interp):
46     return 3*(1+interp(np.exp(loga)))
47
48 # Resolution in the time domain:
49 a_resolution = 3000
50
51 # Resolution in discretization of values of w0
52 w0_resolution = 100
53
54 a_values = np.logspace(-14, 0, a_resolution) # Corresponding to the
    time domain in CLASS
55
56 np.savetxt("temp_scalefactors.csv", a_values.T, delimiter=",", fmt="
    %.16f")
57
58 smallest = 0.0001
59 largest = 0.0005
60
61 w0_values = np.linspace(smallest, largest, w0_resolution)
62 #             ^             ^ Biggest w0 in the dataset
63 #             \             / Smallest w0 in the dataset
64
65 equations_of_state = []
66 derivatives = []
67 interpolators = []
68
69 time1 = time.time()
70
71 # Compute w(a) and w'(a) for given w0, and a in the domain E-14 to 1
72 for WW in w0_values:
73     w_values = []
74     der_values = []
75     for AA in a_values:
76         temp_w=solve_for_w(AA,WW,WW)
77         w_values.append(temp_w)
78         if temp_w == 1:
79             der_values.append(0)
80         else:
81             der_values.append(-3*temp_w*temp_w*(1+temp_w)/AA)
82     equations_of_state.append(w_values)
83     derivatives.append(der_values)
84     interpolators.append(interp1d(a_values, w_values, kind='linear'))
85 time2 = time.time()
86
87 print("Done computing w, w', and storing interpolators")
88 print("{:.2f} seconds".format(time2-time1))
89

```

```

90 np.savetxt("w.csv", np.array(equations_of_state).T, delimiter=",", fmt=
    "%.6f")
91 np.savetxt("w_derivative.csv", np.array(derivatives).T, delimiter=",",
    fmt="%.6f")
92
93 print("Exported CSV file with w values and CSV file with w'(a) values."
    )
94
95 # Now that we computed w(a) and created interpolators,
96 # it is straightforward to compute the integral
97
98 integrals = []
99
100 interpolator_counter = 0
101 time3 = time.time()
102 for WW in w0_values:
103     integral_values = []
104     for AA in a_values:
105         integral_values.append(integrate_function_interpolatedlog(
106             function_to_integrate_interpolatedlog,
107                                     AA,
108                                     interpolators[interpolator_counter]
109                                     )
110         )
111         integrals.append(integral_values)
112         interpolator_counter = interpolator_counter + 1
113 time4 = time.time()
114 print("Done computing integrals")
115 print("{:.2f} seconds".format(time4-time3))
116
117 np.savetxt("integrals.csv", np.array(integrals).T, delimiter=",", fmt="
    "%.6f")
118 #np.savetxt("integrals.dat", np.array(integrals).T, delimiter=" ",
    fmt="%.6f")
119
120
121 # Find longest line length in all the files
122 def longest_line_length(filepath):
123     with open(filepath, 'r', encoding='utf-8') as f:
124         return max(len(line.rstrip('\n')) for line in f)
125
126 longest_line_length = max([longest_line_length("w.csv"),
127                             longest_line_length("w_derivative.csv"),
128                             longest_line_length("integrals.csv")])
129
130 # Output console message
131 print("Integrals exported as CSV")
132 print("Modify the SCDM CLASS code to work with")
133 print("")
134 print("")
135 print("#define N "+str(w0_resolution))
136 print("#define ROWS "+str(a_resolution))
137 print("#define LINE_LENGTH "+str(longest_line_length)+" (at least!)")
138 print("")
139 print("double data_upper_bound = "+str(largest)+";")
140 print("double data_lower_bound = "+str(smallest)+";")

```

```
141 print("")
142 print("")
143 print("these modifications goe inside background.c")
```